OPEN ACCESS
Journal of Innovative Optical Health Sciences
Vol. 14, No. 5 (2021) 2143001 (8 pages)

DOI: 10.1142/S179354582143001X

World Scientific
www.worldscientific.com

Varying of up-conversion nanoparticles luminescence from the muscle tissue depth during the compression

Marina Kozintseva[*,‡,§], Vyacheslav Kochubey[*,†,¶], Julia Konyukhova[*] and Valery Tuchin[*,†]

[*]*Saratov State University, 83, Astrakhanskaya st. Saratov 410012, Russia*

[†]*Tomsk State University, 36, Lenin Avenue Tomsk 634050, Russia*

[‡]*Tsinghua - Berkeley Shenzhen Institute Building C2&C3, Zhiyuan No. 1001 Xueyuan Avenue Nanshan District, Shenzhen, P. R. China*

[§]*marin15121991@mail.ru*

[¶]*saratov_gu@mail.ru*

Received 6 July 2021
Accepted 6 July 2021
Published 18 August 2021

The current work is focused on the study of optical clearing of skeletal muscles under local compression. The experiments were performed on *in vitro* bovine skeletal muscle. The time dependence of optical clearing was studied by monitoring the luminescence intensity of $NaYF_4$: Er,Yb upconverting particles located under tissue layers. This study shows the possibility to use upconverting nanoparticles (UCNPs) both for studying the dynamics of the optical clearing of biological tissue under compression and to detect moments of cell wall damage under excessive pressure. The advantage of using UCNPs is the presence of several bands in their luminescence spectra, located both at close wavelengths and far apart.

Keywords: Upconverting particle; biological tissue; skeletal muscle tissue; tissue optical clearing; luminescence imaging technique; mechanical compression.

1. Introduction

At the present day, noninvasive methods of diagnostics and therapy of various diseases are being intensively developed in medicine. The last decades have seen a massive interest in research in the field of interaction of light with biological tissues of the human body. There are many varieties of optical imaging techniques suitable for studying the

¶Corresponding author.

biological and optical properties of tissues. Such research offers opportunities to manipulate these properties and to develop new therapies that are suitable for clinical use. This knowledge reveals the possibilities to control these properties and to discover new treatment methods, which will be suitable for clinical application.

Within biological tissue, light is attenuated through absorption and scattering. Biotissues are heterogeneous materials and have various components. Some of the major tissue light absorbers are water, blood, and lipids. Several so-called transparency windows with low light absorption by biological macromolecules and water and suitable for diagnostic and therapeutic purposes can be distinguished. Scattering occurs at inhomogeneities of the refractive index (RI) of various components. In general, for biological tissues, values of the scattering coefficient are much higher than those of the absorption coefficient.[1]

Using skeletal muscle as an example, consider why the scattering coefficient is so high. Skeletal muscle is a fibrous tissue that contains actin and myosin fibers. The fibers are grouped in fiber cords. The space between the fiber cords is filled with the interstitial fluid, which is composed mainly of water and some dissolved salts and proteins.[1] At 589.6 nm, the RI of the interstitial fluid usually ranges between 1.35 and 1.37,[2] and the RI of hydrated proteins is of the order of 1.53.[3] The considerable mismatch between the RIs of the fiber cords and the interstitial fluid causes multiple scattering and poor transmittance of light.[2,4,5] As a result, the radiation penetration depth decreases.

Various methods of reducing light scattering in tissues are proposed. One of them is the optical immersion of tissues in exogenous hyperosmotic chemical agents.[1] To minimize light scattering in biological tissues, it is necessary to change the RI of the tissue fluids, raising it to approximate the RI of tissue scatterers. As a clearing agent, a harmless liquid with a RI higher than that of water is used, better matched to the RI of other components of the tissue. Since these agents are hyperosmotic, the interstitial fluid fluxes out of the tissue, dehydrating it, and the agent almost simultaneous diffuses into the tissue. This provides the RI matching mechanism.[6,7] As a result, tissue transparency is increased.[8] Both the tissue dehydration and RI matching are reversible.[1]

In Ref. 9, it is shown that optical clearing makes it possible to increase the probing depth and image quality through the reduction of light scattering in biological tissue. The optical clearing method can be used for optical imaging and diagnostics *in vivo*. To visualize the biological tissue structure and determine the dynamics of the clearing process, one can use: confocal microscopy,[10] two-photon microscopy,[11,12] transmitted-light registration, optical projection tomography, registration of autofluorescence of biological tissue or fluorescence of specially introduced dyes or nanoparticles, nonlinear and Raman microscopy.[13]

A review of biotissue clearing methods for fluorescence imaging of deep tissue areas is given in Ref. 14. Tissue autofluorescence, *in vivo* fluorescent labels, endogenous fluorescence, and *ex vivo* immunolabeling are applied for *in situ* 3D imaging of morphological and functional features of unsectioned whole-mount tissue samples.

Visualization of biological tissue can be used not only to determine its structure, but also to study the processes of optical clearing. In Ref. 15, a highly sensitive laser speckle imaging system and fluorescent intravital microscopy were used to study the skin vascular permeability reaction in mouse ear during the local application of an optical clearing agent on the skin surface. The obtained results suggest that this technique is highly effective for monitoring cutaneous vascular permeability and can be used to assess allergic reactions of the skin when it interacts with chemicals.

Using sequential optical coherence tomography imaging of mouse skull samples during the clearing process, the efficiency of reversible optical clearing was evaluated *in vitro* and *in vivo* for minimally invasive longitudinal imaging of the rodent brain.[16] Different clearing agents were used to study optical clearing processes *in vitro*. The dynamics of clearing with various clearing agents was also studied using two-photon microscopy.[17]

The injection of osmotically active substances into a sample leads to changes in the shape and size of structural elements, though. Furthermore, the injection of an immersion agent in a biotissue *in vivo* is difficult because of the homeostasis of living systems.

Another effective method of controlling the optical properties of biological tissues is local mechanical compression.[18–30] The amount of scattering in a tissue depends not only on the RI mismatch, but also on the concentration and spacing of scatterers. Under mechanical compression, the

interstitial water and blood fractions decrease in the compressed region. This leads to a RI matching, which in turn causes a decrease in the average light scattering. Eventually, tissue transmittance increases and tissue reflectance decreases.[1] On the other hand, compression decreases sample thickness (up to 78%),[19] which leads to an increase in the effective concentration of scattering centers and chromophores inside the tissue. This causes a certain increase in the absorption and scattering coefficients. But a significant decrease in sample thickness compensates for certain elevations of these coefficients, providing an increase in the transmitted light intensity.[1]

Analysis of the image dynamics in clearing made it possible to study the contributions of various processes (lipid removal, size change, and matching of the RI between the imaging solution and the tissue).[31]

The dynamics of changes in transmission of biological tissues *in vitro* can be studied by collimated transmission measurements.[2] However, this mode is not available for *in vivo* studies and medical application. One solution to this problem is to measure the luminescence intensity from nanoparticles embedded in biological tissue. The use of nanoparticles for obtaining luminescent images makes it possible to study the dynamics of not only biotissue clearing, but also the penetration of nanoparticles into tissues and their spatial distribution.[32]

Upconverting nanoparticles (UCNPs) are highly promising for visualizing the structure of deep biological tissues in luminescent light. UCNPs are capable of converting long-wavelength exciting radiation into short-wavelength luminescent radiation.[33–35] In this case, the background autofluorescence of tissues in the spectral region of recording upconversion luminescence is significantly reduced. The illumination from the pump laser can usually be almost completely suppressed by using additional spectral filters. Application of infrared light (in a tissue optical transparency window) for the excitation of UCNPs makes them suitable for *in vivo* deep imaging, as confirmed by many studies.[33,34,36–40]

The aim of this work is to study optical clearing of skeletal muscles under local compression. The time course of clearing was determined from the time dependence of the luminescence intensity of nanoparticles located deep in a tissue layer. Experiments should take into account the size, shape, and distribution of muscle fibers relative to the long axis of the muscle and the direction of compression.

2. Materials and Methods

2.1. *Materials*

The following experiments were performed on bovine skeletal muscle specimens *in vitro*. The eight specimens with the average thickness of $\langle 1.174 \pm 0.134 \rangle$ mm before clearing were used. Muscle tissue was sliced along the fibers, so the fibers were arranged parallel to each other. All the tissue specimens were about $20 \times 20\,\text{mm}^2$ in size. Adipose tissue was removed.

To record the time course of clearing, we used $NaYF_4$:Er,Yb UCNPs synthesized in-house. The nanoparticles were embedded in cellulose acetate film. The room temperature luminescence spectrum of these nanoparticles is shown in Fig. 1.

2.2. *Methods*

Figure 2 represents the schematic diagram of the experimental setup. UCNPs were excited using a LSR980NL-1W laser diode (980 nm) (Lasever, China) with an output of 0.5 W power. Luminescence spectra were recorded using a fiber optic spectrometer (Ocean Optics QE65000 FL, USA). The excitation beam was supplied, the luminescence was collected using a R400-7-VIS/NIR fiber optic probe (Ocean Optics, USA) coupled with the laser and the spectrometer. Diameter of the probe end is 6.2 mm, and the optical fibers are arranged as shown in Fig. 2(b). The fiber diameter is 400 μm. Excitation light was provided from a central fiber. Luminescence was collected by six peripheral fibers.

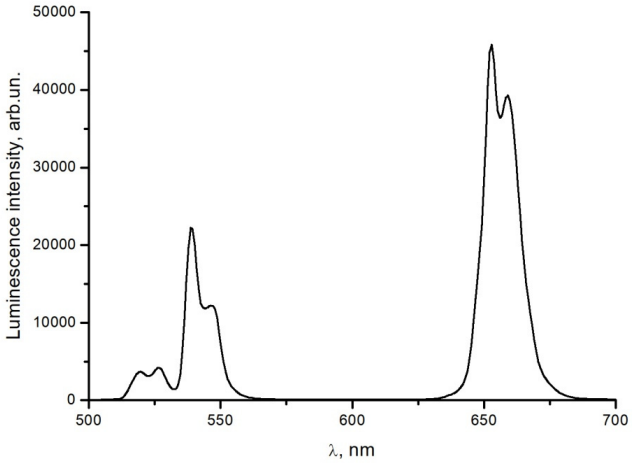

Fig. 1. Luminescence spectrum of $NaYF_4$:Er,Yb nanoparticles embedded in cellulose acetate film (without muscle tissue) under 980 nm excitation. Relative intensities are shown in arbitrary units.

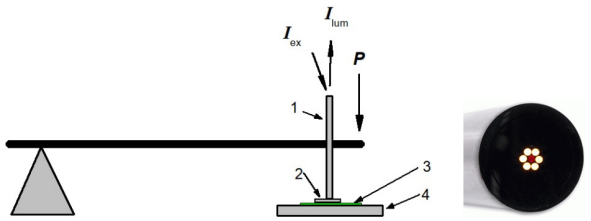

(a) (b)

Fig. 2. (a) Schematic diagram of the experimental setup: (1) fiber optic probe, (2) muscle tissue specimen, (3) cellulose acetate film with embedded $NaYF_4$:Er,Yb UCNPs, (4) fixed base. (b) Image of the probe end.

Cellulose acetate film with embedded $NaYF_4$:Er, Yb UCNPs was placed on a fixed base. A muscle tissue specimen was disposed directly on the film. Pressure on the muscle tissue specimen was carried out using the fiber optic probe. The probe was rigidly fixed to a lever, at the end of which weights were suspended, thus creating the necessary pressure. The pressure was applied to the tissue specimen by the bottom side of the probe. External pressure was increased gradually from 80 kPa to 560 kPa by adding a weight every 10 min.

UCNP luminescence was detected through a muscle tissue specimen layer. The luminescence spectra were recorded with an interval of 3 min.

Specimen thicknesses were measured before and after the experiment was completed and the pressure was released.

3. Results and Discussion

Table 1 lists examples of the thickness decreasing due to compression.

By the way of illustration, Fig. 3 shows UCNP luminescence spectra recorded at the time of changing the pressure applied to the muscle tissue specimen No. 4. The recorded luminescence intensity of the nanoparticles increases with increasing pressure.

Table 1. Thicknesses of the skeletal muscle tissue specimens.

	Before compression clearing		After compression clearing	
Specimen No	Thickness (mm)	Standard deviation (mm)	Thickness (mm)	Standard deviation (mm)
1	1.24	0.01	0.82	0.026
2	1.33	0.01	1.05	0.044
3	1.08	0.01	0.8	0.04
4	1.045	0.005	0.85	0.025
Average thickness	⟨1.174⟩	0.134	⟨0.88⟩	0.114

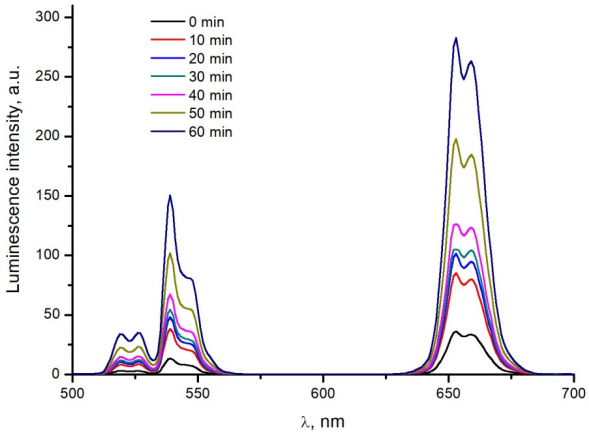

Fig. 3. Time dependence of the luminescence spectrum of $NaYF_4$:Er,Yb nanoparticles embedded in cellulose acetate film, recorded in the process of compression of muscle tissue (specimen No. 4). Excitation of wavelength equal to 980 nm was used. Relative intensities are shown in arbitrary units.

Using the obtained luminescence spectra, $NaYF_4$:Er,Yb nanoparticle luminescence intensity at individual wavelengths was plotted as a function of time of pressure application to the muscle tissue specimens (see Fig. 4). The black vertical lines point to the weight change moments.

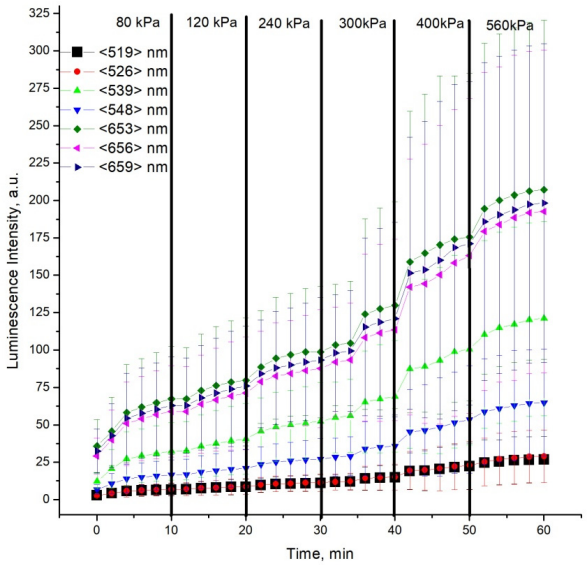

Fig. 4. Intensity of $NaYF_4$:Er,Yb nanoparticle luminescence at individual wavelengths as a function of time of pressure application to the muscle tissue specimens. The moments of pressure change are marked with black thick vertical lines. The thin vertical lines show the standard deviation values. Relative intensities are shown in arbitrary units.

The dynamics of luminescence intensity changes in the recorded spectra is obvious. The increase of the intensity within the first 4 min is clearly seen. Then, regardless of pressure, the intensity increases slowly up to a pressure of 300 kPa. At high pressures, a sharp increase in the luminescence signal is observed at approximately 35, 40 and 50 min, followed by a slow increase in the luminescence intensity. In our opinion, at pressures of 300 kPa and higher, destruction of the cell walls can happen, which leads to a sharp decrease in the specimen thickness.

The observed changes could have been caused by a decrease in both absorption and scattering of light in the muscle tissue specimens. The reduction of the attenuation of the luminescence signal could be the result of a decrease in the total amount of absorbing centers in the optical path, or shortening the optical path due to a decrease in scattering.

We also studied the time dependence of the upconversion luminescence intensity of $NaYF_4$:Er, Yb nanoparticles, provided that pressure was applied directly to the cellulose acetate film (without tissue specimen). The experimental conditions were similar to those for muscle tissue. The experiment showed that the luminescence intensity does not depend on the amount of pressure applied and the compression duration. The signal instability did not exceed 5%, which corresponds to the nameplate instability of the power of the laser used.

For the model of infinite cylinders, the scattering coefficient μ_s of a tissue is defined by the following equation[41,42]:

$$\mu_s = \frac{f_s}{\pi a^2}\,\frac{(1-f_s)^3}{1+f_s} * \sigma_s, \tag{1}$$

where a is the scatterer radius, σ_s is the scattering cross section, and f_s is the volume fraction of tissue scatterers. In our case:

$$f_s + f_w = 1,$$

where f_w is the volume fraction of the interstitial water.

The scattering cross section is determined by the ratio of the refractive indices of collagen fibrils (n_c) and the interstitial fluid (n_w)[43]:

$$\sigma_s = \frac{\pi^2 a x^3}{8}(m^2-1)^2\left(1+\frac{2}{(m^2+1)^2}\right), \tag{2}$$

where $x = 2\pi a n_w/\lambda_0$ is the diffraction parameter, λ_0 is the wavelength of the incident light in a vacuum, and $m = n_c/n_w$ is the relative RI of the scatterers.

Table 2. RIs of the interstitial fluid (n_w), muscle tissue (n_m), and muscle fibers (n_c) at different wavelengths.

λ (nm)	n_w	n_m	n_c
480	1.3557	1.37592	1.44597
486	1.35683	1.37569	1.441
546	1.35307	1.37385	1.44586
589	1.3517	1.37293	1.44648
644	1.3508	1.37205	1.44569
656	1.35047	1.3719	1.44614
800	1.34743	1.37059	1.45081
1100	1.34163	1.36944	1.46575

We experimentally determined the RI of the interstitial fluid (n_w) using a DR-M2/1550 refractometer (Atago, Japan) with interference filters with center wavelengths of 480, 486, 546, 589, 644, 656, 680, 800, 930, and 1100 nm (see Table 2). The RI of muscle tissue (n_m) was calculated using the Cauchy equation[1]:

$$n_m = A + \frac{B}{\lambda^2} + \frac{C}{\lambda^4}. \tag{3}$$

Values of the dispersion coefficients A, B, and C were taken from Ref. 44. Using the Gladstone–Dale law and assuming the volume fraction of muscle fibers (f_c) equal to 0.244 ± 0.003,[45] the RI of muscle fibers (n_c) was calculated:

$$n_c(\lambda) = \frac{n_m(\lambda) - n_w(\lambda)(1-f_c)}{f_c}. \tag{4}$$

Calculated values of RIs for muscle tissue and muscle fibers are listed in Table 2.

The obtained values of (n_c) are less than those indicated for dry muscle fibers (1.584).[46,47] Obviously, this is caused by the presence of water in the fibers of the specimens under study.

When the specimen is compressed and tissue cells are not destroyed, the amount of the interstitial fluid in the specimen decreases, but its composition does not change. Consequently, the scattering cross section does not change, and changes in the scattering coefficient should be caused by a change in the volume fraction of the scatterers in the tissue. In this case, the relative change in the luminescence intensity at different wavelengths should be the same, if the removal of the fluid is not accompanied by a change in the absorption coefficient. Based on the results from Table 2, we have calculated the relative RI (m) for the wavelengths shown in the table. The value of the relative RI varies slightly with wavelength (within 1.06–1.07). At the same

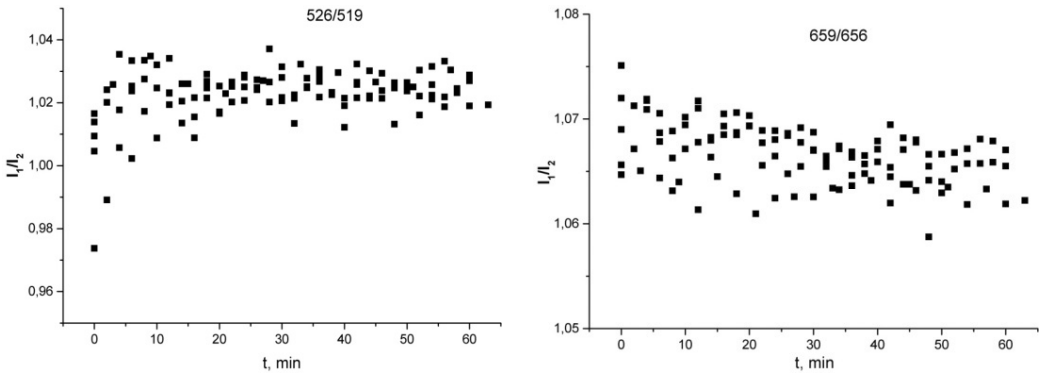

Fig. 5. Intensity ratios of the UCNP luminescence bands peaking at (a) 526 and 519 nm and (b) 659 and 656 nm versus time of pressure application to the muscle tissue specimens.

time, the absorption coefficient is small in the 520–530 and 600–650 nm ranges and rather large in the 540–560 nm range due to the absorption of hemoglobin.

We analyzed the behavior of the intensity ratios of the UCNP luminescence in the spectral regions of strong and weak absorption. For the case of weak absorption, in Fig. 5 the intensity ratios (I_1/I_2) of luminescence bands peaking at 526 and 519 nm in Fig. 5(a) and at 659 and 656 nm in Fig. 5(a) have been plotted as a function of time of pressure application to the muscle tissue specimens. In Fig. 6, similar dependences are plotted for luminescence bands peaking at 548 and 656 nm (the regions of strong and weak absorption, respectively).

It is apparent from Fig. 5 that applying pressure does not affect the luminescence intensity ratio. This does not happen even after the application of pressure, which, in our opinion, leads to the destruction of the cell walls and a sharp clearing of the tissue. This is because the intracellular fluid has the same RI as the interstitial fluid. In this case, a sharp clearing occurs due to a change in the specimen thickness during cell deformation.

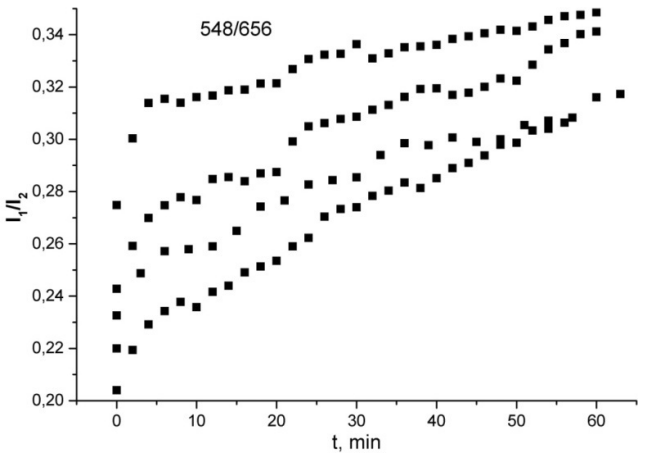

Fig. 6. Intensity ratios of the UCNP luminescence bands peaking at 548 and 656 nm versus time of pressure application to the muscle tissue specimens.

It is apparent from Fig. 6 that the clearing occurs faster at 548 nm than at 656 nm. This is due to the change in absorption at 548 nm due to the removal of hemoglobin. The difference in the dependences for different specimens is explained by the difference in their thickness. Similar to Fig. 5, no change in the dynamics of the dependences is observed when the threshold of cell destruction is exceeded.

4. Conclusion

It has been shown that the proposed technique using UCNPs is suitable for studying the dynamics of the optical clearing of biological tissue under external pressure. It is also possible to register the moment of destruction of the cell walls when the required pressure is reached. The technique makes it possible to monitor separately the clearing caused by pressure and due to the change in absorption in the sample. To do this, you need to choose different wavelengths. The advantage of using UCNPs is the presence of several bands in their luminescence spectra, located both at close wavelengths and far apart.

Conflict of Interest

The authors declare to have no conflict of interest.

Acknowledgment

This work was supported by the Russian Science Foundation, project no. 19-12-00118.

References

1. L. Oliveira, V. V. Tuchin, *The Optical Clearing Method: A New Tool for Clinical Practice and Biomedical Engineering*, Springer Nature Switzerland AG, Basel (2019).
2. V. V. Tuchin, *Optical Clearing of tissues and blood*, SPIE Press, Bellingham, WA (2006).
3. W. L. Bragg, A. B. Pippard, "The form birefringence of macromolecules," *Acta Cryst.* **6**, 865–867 (1953).
4. V. V. Tuchin, *Tissue Optics: Light Scattering Methods and Instruments for Medical Diagnosis*, SPIE Press, Bellingham (2015).
5. A. N. Bashkatov, E. A. Genina, V. V. Tuchin, "Optical properties of skin, subcutaneous, and muscle tissues: A review," *J. Innov. Opt. Health Sci.* **4**(1), 9–38 (2011).
6. L. Oliveira, M. I. Carvalho, E. Nogueira, V. V. Tuchin, "Optical clearing mechanisms characterization in muscle," *J. Innov. Opt. Health Sci.* **9**(5), 1650035 (2016).
7. L. Oliveira, M. I. Carvalho, E. M. Nogueira, V. V. Tuchin, "Diffusion characteristics of ethylene glycol in skeletal muscle," *J. Biomed. Opt.* **20**(5), 051019 (2015).
8. E. A. Genina, A. N. Bashkatov, V. V. Tuchin, "Tissue optical immersion clearing," *Expert Rev. Med. Dev.* **7**(6), 825–842 (2010).
9. E. A. Genina, A. N. Bashkatov, Yu. P. Sinichkin, I. Yu. Yanina, V. V. Tuchin, "Optical clearing of biological tissues: prospects of application in medical diagnostics and phototherapy," *J. Biomed. Photon. Eng.* **1**(1), 22–58 (2015).
10. A. Gerger, S. Koller, T. Kern, C. Massone, K. Steiger, E. Richtig, H. Kerl, J. Smolle, "Diagnostic applicability of in vivo confocal laser scanning microscopy in melanocytic skin tumors," *J. Invest. Dermatol.* **124**, 493–498 (2005).
11. R. Cicchi, F. S. Pavone, D. Massi, D. D. Sampson, "Contrast and depth enhancement in two-photon microscopy of human skin ex vivo by use of optical clearing agents," *Opt. Exp.* **13**, 2337–2344 (2005).
12. S.-J. Tseng, Y.-H. Lee, Z.-H. Chen, H.-H. Lin, C.-Y. Lin, S.-C. Tang, "Integration of optical clearing and optical sectioning microscopy for three-dimensional imaging of natural biomaterial scaffolds in thin sections," *J. Biomed. Opt.* **14**(4), 044004 (2009).
13. D. Huang, W. Zhang, H. Zhong, H. Xiong, X. Guo, Z. Guo, "Optical clearing of porcine skin tissue in vitro studied by Raman microspectroscopy," *J. Biomed. Opt.* **17**(1), 015004 (2012).
14. A. Feuchtinger, A. Walch, M. Dobosz, "Deep tissue imaging: a review from a preclinical cancer research perspective," *Histochem. Cell Biol.* **146**, 781–806 (2016).
15. V. Kalchenko, I. Meglinski, A. Sdobnov, Y. Kuznetsov, A. Harmelin, "Combined laser speckle imaging and fluorescent intravital microscopy for monitoring acute vascular permeability reaction," *J. Biomed. Opt.* **24**(6), 060501 (2019).
16. H. Soleimanzad, M. Juchaux, H. Gurden, D. Crepin, F. Pain, "Evaluation of skull optical clearing process for longitudinal non invasive optical imaging," *Proc. SPIE* **11226**, 1122614 (2020).
17. L. Deng, W. Feng, T. Yu, D. Zhu, "In vivo monitoring optical clearing process of skin using two-photon microscopy," *Proc. SPIE* **10820**, 108203E (2018).
18. C. G. Rylander, O. F. Stumpp, T. E. Milner, N. J. Kemp, J. M. Mendenhall, K. R. Diller, A. J. Welch, "Dehydration mechanism of optical clearing in tissue," *J. Biomed. Opt.* **11**(4), 041117 (2006).
19. E. K. Chan, B. Sorg, D. Protsenko, M. O'Neil, M. Motamedi, A. J. Welch, "Effects of compression on soft tissue optical properties," *IEEE J. Select. Top. Quant. Electron.* **2**(4), 943–950 (1996).
20. W. Chen, R. Liu, K. Xu, R. K. Wang, "Influence of contact state on NIR diffuse reflectance spectroscopy in vivo," *J. Phys. D: Appl. Phys.* **38**, 2691 (2005).
21. R. Reif, M. S. Amorosino, K. W. Calabro, O. A'Amar, K. S. Singh, I. J. Bigio, "Analysis of change in reflectance measurements on biological tissues subjected to different probe pressures," *J. Biomed. Opt.* **13**(1), 010502 (2008).
22. C. G. Rylander, T. E. Milner, S. A. Baranov, J. S. Nelson, "Mechanical tissue optical clearing devices: Enhancement of light penetration in *ex vivo* porcine skin and adipose tissue," *Laser Surg. Med.* **40**(10), 688–694 (2008).
23. W. C. Vogt, H. Shen, G. Wang, C. G. Rylander, "Parametric study of tissue optical clearing by localized mechanical compression using combined finite element and Monte Carlo simulation," *J. Innov. Opt. Health Sci.* **3**(3), 203–211 (2010).
24. R. A. Izquierdo, W. C. Vogt, L. Hyacinth, C. G. Rylander, "Mechanical tissue optical clearing technique increases imaging resolution and contrast through *ex vivo* porcine skin," *Laser Surg. Med.* **43**, 814–823 (2011).
25. A. Gurjarpadhye, W. C. Vogt, Y. Liu, C. G. Rylander, "Effect of localized mechanical indentation on skin water content evaluated using OCT," *Int. J. Biomed. Imaging.* **2011**, 817250 (2011).
26. W. C. Vogt, A. Izquierdo-Roman, B. Nichols, L. Lim, J. W. Tunnell, C. G. Rylander, "Effects of

mechanical indentation on diffuse reflectance spectra, light transmission, and intrinsic optical properties in *ex vivo* porcine skin," *Laser Surg. Med.* **44**, 303–309 (2012).
27. C. Li, J. Jiang, K. Xu, "The variations of water in human tissue under certain compression: Studied with diffuse reflectance spectroscopy," *J. Innov. Opt. Health Sci.* **6**(1), 1350005 (2013).
28. I. A. Nakhaeva, R. M. Mohammed, O. A. Zyuryukina, Yu. P. Sinichkin, "Effect of external mechanical pressure on optical properties of the human skin in vivo," *Opt. Spectrosc.* **117**(3), 506–512 (2014).
29. I. A. Nakhaeva, R. M. Mohammed, O. A. Zyuryukina, Yu. P. Sinichkin, "The effect of external mechanical compression on in vivo water content in human skin," *Opt. Spectrosc.* **118**(5), 834–840 (2015).
30. O. A. Zyuryukina, Yu. P. Sinichkin, "The dynamics of optical and physiological characteristics of human skin in vivo during its compression," *Opt. Spectrosc.* **127**(3), 555–561 (2019).
31. J. H. Kim, M. J. Jang, J. Choi, E. Lee, K. D. Song, J. Cho, K. T. Kim, H. J. Cha, W. Sun, "Optimizing tissue-clearing conditions based on analysis of the critical factors affecting tissue-clearing procedures," *Sci. Rep.* **8**(1), 12815 (2018).
32. L. Yang, R. Gradl, M. Dierolf, W. Möller, D. Kutschke, A. Feuchtinger, L. Hehn, M. Donnelley, B. Günther, K. Achterhold, A. Walch, T. Stoeger, D. Razansky, F. Pfeiffer, K. S. Morgan, O. Schmid, "Multimodal precision imaging of pulmonary nanoparticle delivery in mice: dynamics of application, spatial distribution, and dosimetry," *Small* **15**(49), 1904112 (2019).
33. K. Huang, N. M. Idris, Y. Zhang, "Engineering of lanthanide-doped upconversion nanoparticles for optical encoding," *Small* **12**(7), 836–852 (2016).
34. A. H. All, X. Zeng, D. B. L. Teh, Z. Yi, A. Prasad, T. Ishizuka, N. Thakor, Y. Hiromu, X. Liu, "Expanding the toolbox of upconversion nanoparticles for in vivo optogenetics and neuromodulation," *Adv. Mater.* **31**, e1803474 (2019).
35. X. Wu, Y. Zhang, K. Takle, O. Bilsel, Z. Li, H. Lee, Z. Zhang, D. Li, W. Fan, C. Duan, "Dye-sensitized core/active shell upconversion nanoparticles for optogenetics and bioimaging applications," *ACS Nano* **10**, 1060–1066 (2016).
36. E. K. Volkova, I. Yu Yanina, E. A. Genina, A. N. Bashkatov, J. G. Konyukhova, A. P. Popov, E. S. Speranskaya, A. B. Bucharskaya, N. A. Navolokin, I. Yu. Goryacheva, V. I. Kochubey, G. B. Sukhorukov, I. V. Meglinski, V. V. Tuchin, "Delivery and reveal of localization of upconversion luminescent microparticles and quantum dots in the skin in vivo by fractional laser microablation, multimodal imaging, and optical clearing," *J. Biomed. Opt.* **23** (2), 026001 (2018).
37. E. K. Volkova, I. Yu. Yanina, E. A. Genina, L. E. Dolotov, A. N. Bashkatov, V. D. Genin, J. G. Konyukhova, A. P. Popov, M. D. Kozintseva, E. Speranskaya, M. Lomova, G. S. Terentyuk, A. B. Bucharskaya, N. A. Navolokin, I. Yu. Goryacheva, V. I. Kochubey, D. A. Gorin, V. V. Tuchin, G. B. Sukhorukov, "Luminescence monitoring of particle delivery into rat skin in vivo," *Proc. SPIE* **9537**, 95371P (2015).
38. M. D. Kozintseva, E. K. Volkova, J. G. Konyukhova, I. V. Zabenkov, V. I. Kochubey, "Luminescence monitoring of temporal changes and efficiency of tissue optical clearing by NIR-excited upconversion particles," *BioNanoScience* **6**, 169–175 (2016).
39. N. Svensson, C. Xu, "Upconverting luminescence imaging and tomography for biomedical applications," Lund Reports on Atomic Physics, LRAP-401 (2008), http://www.atomic.physics.lu.se/biophotonics.
40. E. A. Shirshin, Y. I. Gurfinkel, A. V. Priezzhev, V. V. Fadeev, J. Lademann, M. E. Darvin, "Two-photon autofluorescence lifetime imaging of human skin papillary dermis in vivo: Assessment of blood capillaries and structural proteins localization," *Sci. Rep.* **7**, 1171 (2017).
41. J. M. Schmitt, G. Kumar, "Optical scattering properties of soft tissue: a discrete particle model," *Appl. Opt.* **37**(13), 2788–2797 (1998).
42. A. N. Bashkatov, E. A. Genina, V. V. Tuchin, Measurement of glucose diffusion coefficients in human tissues, *Handbook of Optical Sensing of Glucose in Biological Fluids and Tissues*, Chap. 19, V. V. Tuchin, Ed., pp. 587–621, Taylor & Francis Group LLC, CRC Press, Boca Raton, London, New York (2009).
43. C. F. Bohren, D. R. Huffman, *Absorption and Scattering of Light by Small Particles*, Wiley, New York (1983).
44. Z. Deng, J. Wang, Q. Ye, T. Sun, W. Zhou, J. Mei, C. Zhang, J. Tian, "Determination of continuous complex refractive index dispersion of biotissue based on internal reflection," *J. Biomed. Opt.* **21**(1), 015003 (2016).
45. L. Oliveira, A. Lage, M. Pais Clemente, V. V. Tuchin, "Optical characterization and composition of abdominal wall muscle from rat," *Opt. Lasers Eng.* **47**, 667–672 (2009).
46. L. Oliveira, M. I. Carvalho, E. Nogueira, V. V. Tuchin, "Skeletal muscle dispersion (400 – 1000 nm) and kinetics at optical clearing," *J. Biophoton.* **11** (1), e201700094 (2018).
47. L. Oliveira, A. Lage, M. Pais Clemente, V. V. Tuchin, "Optical characterization of muscle," *Proc. SPIE* **8337**, 833705 (2011).